Representing sub-grid scale variations in nitrogen deposition associated with land use in a global Earth System Model: implications for present and future nitrogen deposition fluxes over North America

Fabien Paulot[1,2], Sergey Malyshev[1], Tran Nguyen[3], John D. Crounse[4], Elena Shevliakova[1], and Larry W. Horowitz[1]

[1]Geophysical Fluid Dynamics Laboratory, National Oceanic and Atmospheric Administration, Princeton, New Jersey, USA
[2]Program in Atmospheric and Oceanic Sciences, Princeton University, New Jersey, USA
[3]Department of Environmental Toxicology, UC Davis, Davis, California, USA
[4]Division of Geological and Planetary Sciences, Caltech, Pasadena, California, USA

Correspondence to: Fabien.Paulot@noaa.gov

Abstract. Reactive nitrogen (N) emissions have increased over the last 150 years as a result of greater fossil fuel combustion and food production. The resulting increase in N deposition can alter the function of ecosystems, but characterizing its ecological impacts remains challenging, in part because of uncertainties in model-based estimates of N dry deposition. Here, we use the Geophysical

5   Fluid Dynamics Laboratory (GFDL) atmospheric chemistry-climate model (AM3) coupled with the GFDL land model (LM3) to estimate dry deposition velocities. We leverage the tiled structure of LM3 to represent the impact of physical, hydrological, and ecological heterogeneities on the surface removal of chemical tracers. We show that this framework can be used to estimate N deposition at more ecologically-relevant scales (e.g., natural vegetation, water bodies) than from the coarse-

10   resolution global model AM3. Focusing on North America, we show that the faster removal of N over forested ecosystems relative to cropland and pasture implies that coarse-resolution estimates of N deposition from global models systematically underestimate N deposition to natural vegetation by 10 to 30% in the Central and Eastern US. Neglecting the sub-grid scale heterogeneity of dry deposition velocities also results in an underestimate (overestimate) of the amount of reduced

15   (oxidized) nitrogen deposited to water bodies. Overall, changes in land cover associated with human activities are found to slow down the removal of N from the atmosphere, causing a reduction in the dry oxidized, dry reduced, and total (wet+dry) N deposition over the contiguous US of 8%, 26%, and 6%, respectively. We also find that the reduction in the overall rate of removal of N associated with land-use change tends to increase N deposition on the remaining natural vegetation

20   and facilitate N export to Canada. We show that sub-grid scale differences in the surface removal

of oxidized and reduced nitrogen imply that projected near-term (2010–2050) changes in oxidized (-47%) and reduced (+40%) US N emissions will cause opposite changes in N deposition to water bodies (increase) and natural vegetation (decrease) in the Eastern US, with potential implications for acidification and ecosystems.

25 ## 1 Introduction

Fossil fuel combustion and food production release reactive nitrogen (N) to the atmosphere (Fowler et al., 2013). Once in the atmosphere, N can be transported over long distances before it is removed by dry and wet deposition, providing greater N inputs to otherwise pristine regions (e.g., national parks, boreal forests) (Paulot et al., 2014; Malm et al., 2016). Since N can be a limiting nutrient,
30 the increase in N deposition may promote ecosystem productivity, (Townsend et al., 1996; Magnani et al., 2007; Pregitzer et al., 2008; Reay et al., 2008; Dezi et al., 2010; Wårlind et al., 2014; Devaraju et al., 2015) especially in boreal regions (Högberg, 2012; Gundale et al., 2014; Fleischer et al., 2015). Increasing N deposition can also cause adverse environmental impacts for terrestrial ecosystems including soil acidification, loss of biodiversity, and eutrophication (Stevens et al., 2004; Bobbink
35 et al., 2010; Sutton et al., 2011; Pardo et al., 2011; Sheppard et al., 2011; Phoenix et al., 2012; Erisman et al., 2013; de Vries et al., 2015; Simkin et al., 2016). In the US, oxidized N deposition is projected to decrease as a result of effective controls on NO emissions, but deposition of reduced N ($NH_x \equiv NH_3 + NH_4^+$), primarily from agricultural emissions of NH_3, is projected to remain elevated or even increase (Dentener et al., 2006; Ellis et al., 2013; Paulot et al., 2013; Lamarque et al., 2013;
40 Li et al., 2016). This raises concerns of irreversible damages to sensitive biomes (Pardo et al., 2011; Meunier et al., 2016; Grizzetti, 2011; Dise, 2011), such as high-elevation lakes (Wolfe et al., 2003; Baron et al., 2012; Lepori and Keck, 2012), and organisms (e.g., lichen (Johansson et al., 2012)).

Significant challenges remain in quantifying the long-term impacts of N deposition on ecosystems in a changing climate (Sutton et al., 2008; Wu and Driscoll, 2010; Phoenix et al., 2012; Högberg,
45 2012; de Vries et al., 2015; Storkey et al., 2015), including uncertainties in the speciation, magnitude and spatial distribution of the N deposition flux itself (Sutton et al., 2008; Ochoa-Hueso et al., 2011; Jickells et al., 2013; Fleischer et al., 2013). Many approaches have been developed to provide high-resolution, ecosystem-relevant estimates of both wet and dry N deposition, including statistical models (Singles et al., 1998; Dore et al., 2007; Weathers et al., 2006; Dore et al., 2012), high-resolution
50 nested chemical transport model ($\simeq 4 \times 4\,km$ (Vieno et al., 2009; Simkin et al., 2016)), and hybrid approaches that combine high-resolution regional chemical transport models with observed N fluxes and atmospheric concentrations (e.g. using the Community Multiscale Air Quality Modeling System (Schwede and Lear, 2014; Bytnerowicz et al., 2015; Williams et al., 2017)). However, the elevated computational requirement associated with high-resolution atmospheric models make
55 such approaches impractical for assessing the long-term impact of N deposition on ecosystems, its

sensitivity to climate change, and ultimately its coupling with the carbon cycle (Smith et al., 2014; Zaehle et al., 2010; Fleischer et al., 2013; Dirnböck et al., 2017; Fleischer et al., 2015). For such questions, estimates of N deposition are generally derived from global models with coarse resolution ($\simeq$ 100km, (Dentener et al., 2006; Lamarque et al., 2013)). This introduces a large uncertainty

60 (Hertel, 2011) in N deposition estimates especially for dry deposition, which can vary over short distances ($\sim$1 km) in response to changes in the physical, hydrological, and ecological state of the surface (Weathers et al., 2000; Hicks, 2006, 2008; De Schrijver et al., 2008; Ponette-González et al., 2010; Templer et al., 2014; Tulloss and Cadenasso, 2015).

The goal of this study is to develop a framework to diagnose ecosystem-specific N dry deposi-

65 tion fluxes within a global chemistry climate model on decadal to centennial time scales. First we describe the coupling of the Geophysical Fluid Dynamics Laboratory (GFDL) land-model (LM3) to the GFDL atmospheric chemistry–climate model (AM3) to represent the impact of natural (e.g., vegetation type, soil and canopy wetness) and man-made (e.g., deforestation, cropping) heterogeneities on dry deposition. We then show that the tiled structure of LM3 can be leveraged to derive N depo-

70 sition on a more ecologically-relevant scale (e.g., deposition on water bodies or natural vegetation). Finally, we discuss how this framework can be used to better represent the impact of land-use change and future trends in N emissions on N deposition.

2 Methods

2.1 Model description

75 We use an updated version of the GFDL AM3 atmospheric chemistry–climate model (Donner et al., 2011; Naik et al., 2013; Paulot et al., 2016) to simulate atmospheric dynamics and chemistry. Except for the treatment of dry deposition, the model configuration is identical to the one recently described by Paulot et al. (2016) and Paulot et al. (2017), including updates to wet deposition and the chemistry of sulfate and nitrate. The horizontal resolution of the model is 200km with 48 vertical levels.

80 In AM3, the surface removal of chemical tracers is calculated using a prescribed monthly climatology of dry deposition velocities (Naik et al., 2013; Paulot et al., 2016). The lack of a dynamic representation of dry deposition reduces the ability of the model to capture the impact of past and future variability in environmental conditions (e.g., drought (Wu et al., 2016), climate change) and land-use change on atmospheric chemistry. We note that these limitations are not specific to AM3

85 but affect all chemical transport models that do not include a comprehensive land model (Ellis et al., 2013; Ran et al., 2017).

Here, we describe the development of a new model, in which dry deposition of gaseous and aerosol species is calculated within the dynamic vegetation model LM3 (Shevliakova et al., 2009; Milly et al., 2014). The combined model will be referred to as AM3-LM3-DD hereafter.

3

90   LM3 is a comprehensive climate land model that includes detailed representations of vegetation dynamics and hydrology and is designed to be run over decadal to century time scales under both historical and future conditions. LM3 can be run both coupled with AM3 and in standalone mode with prescribed meteorological fields (Milly et al., 2014).

    In LM3, the heterogeneity of the land surface and vegetation is represented using a sub-grid mo-
95 saic of tiles (Shevliakova et al., 2009; Malyshev et al., 2015) as illustrated in Fig. 1. Each tile has distinct energy and moisture balances for a vegetation–snow–soil column, biophysical properties, and exchanges of radiant and turbulent fluxes with the overlying atmosphere. LM3 predicts physical, biogeochemical, and ecological characteristics for each sub-grid land surface tile from the top of the vegetation canopy to the bottom of the soil column, including leaves and canopy temperature,
100 canopy-air specific humidity, stomatal conductance, snow cover and depth, runoff, vertical distribution of soil moisture, ice, and temperature. The land-use history is prescribed from the Hurtt et al. (2011) reconstruction for each grid cell in terms of annual transition rates among four distinct land-use types: undisturbed (hereafter referred to as natural), crops, pastures, and secondary vegetation. Secondary vegetation is defined in LM3 as the vegetation recovering after land-use and land-cover
105 changes and not currently managed. This includes all abandoned agricultural land as well as the land where wood was harvested at least once in prior years. The model keeps track of different recovery states by creating a secondary vegetation tile every time a disturbance occurs and simulating the subsequent vegetation regrowth in the tile. To avoid unrestricted growth of the number of tiles, the number of secondary vegetation tiles is limited to 10 per grid cell in the configuration of LM3 used
110 here. When more than 10 secondary vegetation titles exist in a grid cell, secondary vegetation tiles with similar properties are merged (Shevliakova et al., 2009), while preserving water, energy, and carbon balances. Land properties that affect the surface removal of chemical tracers, such as snow cover, canopy liquid water and snow mass, surface and canopy temperature, leaf area index (LAI), stomatal conductance, and vegetation height are all prognostic (Shevliakova et al., 2009). Vegetation
115 carbon is partitioned into five pools: leaves, fine roots, sapwood, heartwood, and labile storage. The model simulates changes in vegetation and soil carbon pools, as well as the carbon exchange among these pools and the atmosphere. The sizes of the pools are modified daily depending on the carbon uptake according to a set of allocation rules. Additionally, the model simulates changes in the vegetation carbon pools due to phenological processes, natural mortality, and fire. LAI is determined by
120 vegetation leaf biomass and specific leaf area, prescribed for each vegetation type. Each vegetated tile has a unique vegetation type (C3 grass, C4 grass, temperate deciduous, coniferous, or tropical vegetation), which is determined based on biogeographical rules that take into account environmental conditions as well as the current state of the vegetation in each tile (Shevliakova et al., 2009). The fraction of the canopy covered by liquid water (f_l) and snow (f_s) are estimated from the intercepted

4

canopy liquid water mass (w_l) and snow mass (w_s) following Bonan (1996):

$$f_i = \left(\frac{w_i}{W_{i,max}}\right)^{\frac{2}{3}} \qquad i \in \{l,s\} \tag{1}$$

where $W_{l,max} = 0.02\,kg\,m^{-2}$ and $W_{s,max} = 0.2\,kg\,m^{-2}$ are the maximum liquid water and snow holding capacities, respectively. If both snow and liquid water are present simultaneously, water and snow are assumed to be distributed independently of each other.

The representation of management practices is important in determining the impact of land-use change on dry deposition, as it affects the vegetation type, and the seasonality of the vegetation cover. In LM3, crop harvesting and pasture grazing are performed annually at the end of the calendar year (Malyshev et al., 2015). Previous work has shown that this treatment contributes to an underestimate of the impact of management on land cover (Malyshev et al., 2015). To address these biases, we make the following modifications. For pasture, we assume that 25% of leaf biomass removed daily by grazing, provided LAI exceeds 2 to avoid overgrazing. This higher grazing frequency and intensity prevent the excessive growth of vegetation biomass on pasture in the tropics and mid latitudes, a problem which was noted in previous versions of LM3 (Malyshev et al., 2015) leading to misclassification of pasture vegetation cover as forests (Malyshev et al., 2015). LM3 does not estimate the cropping schedule (e.g., Bondeau et al. (2007)), so we specify planting and harvesting dates from the global monthly irrigated and rainfed crop areas climatology (Portmann et al., 2010). The impact of management practices on the timing and magnitude of agricultural emissions (e.g., Paulot et al. (2014)) is not accounted for in AM3-LM3-DD.

The tiled structure of LM3 is especially useful to diagnose fluxes to areas, such as natural vegetation or water bodies, which are generally not well-represented by the average properties of the grid-box, in which they are located, because of their small geographical extent (Fig. S1).

The dry deposition velocity ($v_d(X)$) for species X is calculated independently for each tile following the widely used electrical circuit analogy (Fig. 1) (Hicks et al., 1987; Wesely, 1989; Zhang et al., 2001, 2003).

$$v_d(X) = \left[R_a + \cfrac{1}{\cfrac{1}{R_{ac,g} + R_{b,g}(X) + R_{sf,g}(X)} + \cfrac{1}{R_{ac,v} + \cfrac{1}{[R_{b,s}+R_{sf,s}]^{-1} + \cfrac{1}{R_{b,v} + \left[R_{sf,v}^{-1} + (R_m + R_s)^{-1}\right]^{-1}}}}}\right]^{-1} \tag{2}$$

Briefly, the aerodynamic resistance (R_a) to the exchange of tracers between the canopy and the atmosphere is determined using Monin-Obukhov similarity theory. The aerodynamic conductance to the ground ($R_{ac,g}$) and to the vegetation ($R_{ac,v}$) are independent of the chemical tracer and taken from Erisman (1994) and Choudhury and Monteith (1988), respectively.

5

$$155 \quad R_{ac,g} = \frac{u_\star}{14(LAI + SAI)h} \tag{3}$$

$$R_{ac,v} = (LAI + SAI) \cdot g_b \text{ with } g_b = 0.01(1 - exp(-3/2)/3)\sqrt{V} \tag{4}$$

where SAI, h, and V are the stem area index, the height of the vegetation, and the normalized wind at the top of the canopy, respectively.

160   We focus next on the representation of the dry deposition of gases, which is much faster than that of fine particles (Zhang et al., 2002).

     Following Jensen and Hummelshøj (1995) and Jensen and Hummelshøj (1997), the canopy laminar resistance ($R_{b,v}$) is defined as:

$$R_{b,v}(X) = \frac{1}{D_X} \left(\frac{u_\star}{\nu} LAI \right)^{-2/3} (100lw)^{1/3} \tag{5}$$

165 where $u_\star$ is the friction velocity, lw the characteristic obstacle length of the canopy (Table S1), ν the kinematic viscosity, and D_X the diffusivity of species X. Following Hicks et al. (1987), the stem laminar resistance is:

$$R_{b,s}(X) = \frac{2}{\kappa u_\star} \left(\frac{Sc(X)}{Pr} \right)^{2/3} \tag{6}$$

where Pr is the Prandtl number, $Sc(X)$ is the Schmidt number, the ratio of the kinematic to the

170 mass diffusivity ($Sc \propto D_X^{-1}$), κ the von Karman constant ($\kappa = 0.4$). Similarly, the ground surface laminar resistance is:

$$R_{b,g}(X) = \frac{2}{\kappa u_{g\star}} \left(\frac{Sc(X)}{Pr} \right)^{2/3} \tag{7}$$

where $u_{g\star}$ is the friction velocity near the ground (Loubet et al., 2006). The stomatal resistance ($R_s(X)$) is calculated as

$$175 \quad R_s(X) = \sqrt{\frac{M(X)}{M(H_2O)}} R_s(H_2O) \tag{8}$$

where $M(X)$ is the molecular weight of species X and $R_s(H_2O)$ is the stomatal resistance for water vapor, calculated according to the Ball-Berry-Leuning model (Leuning, 1995; Milly et al., 2014). This model accounts for the impact of water stress and CO_2 concentration, which have been shown to modulate the response of surface ozone to drought (Huang et al., 2016) and CO_2 increase (Sanderson

180 et al., 2007). Cuticle (v), stem (s), and ground (g) resistances for species X are parameterized based on SO_2 and O_3:

6

$$R_{sf,i}(X) = \frac{s(T)}{\gamma(X)} \left(\frac{\alpha(X)}{R_{sf,i}(\text{SO}_2)} + \frac{\beta(X)}{R_{sf,i}(\text{O}_3)} \right)^{-1} \qquad i \in \{\text{v, s, g}\} \tag{9}$$

where $R_{sf,i}(\text{SO}_2)$ and $R_{sf,i}(\text{O}_3)$ are tabulated resistances (Table S1) for each surface type, and $\alpha(X)$ and $\beta(X)$ are weighting factors (Table S2) estimated using the solubility (for α) and reactivity (for β) of X (Wesely, 1989; Zhang et al., 2002), $s(T)$ is a temperature adjustment factor (Zhang et al., 2003), and $\gamma(X)$ is a codeposition adjustment, which reflects changes in $R_{sf,i}(X)$ associated with surface acidity (Erisman et al., 1994; Massad et al., 2010; Neirynck et al., 2011; Wu et al., 2016). Here, we use the parameterizations of Massad et al. (2010) for NH_3 and Simpson et al. (2003) for SO_2:

$$\gamma(X) = \begin{cases} \exp(2 - r_{SN}) & X = \text{SO}_2 \text{ and } \alpha_{SN} \leq 2 \\ 6.35 r_{SN} & X = \text{NH3} \\ 1 & \text{otherwise} \end{cases} \tag{10}$$

To improve numerical stability, we estimate the acid ratio (r_{SN}) using the ratio of the 24-hour integrated total dry deposition of acids to the dry deposition of ammonia and ammonium, rather than using the ratio of their surface concentrations (Massad et al., 2010; Simpson et al., 2003).

The bidirectional exchange of ammonia is not represented in AM3-LM3-DD (Massad et al., 2010; Flechard et al., 2013). This reflects in part uncertainties in the emission potential of vegetation and the lack of detailed treatment of agricultural activities in LM3 (Riddick et al., 2016). We thus expect AM3-LM3-DD to overestimate NH_3 dry deposition in source regions (Zhu et al., 2015; Sutton et al., 2007).

2.2 Experimental design

We perform two sets of global simulations representative of present-day (circa 2010) and future (2050) conditions. For present-day conditions, AM3-LM3-DD is run from 2007 to 2010 using 2007 as spin-up. The model is forced with observed sea surface temperatures and sea ice cover, and land use from the Representative Concentration Pathways 8.5 scenario (RCP8.5, Riahi et al. (2011)). Anthropogenic emissions are from the Hemispheric Transport of Air Pollution 2 (HTAPv2, Janssens-Maenhout et al. (2015)). Natural emissions are based on Naik et al. (2013), except for isoprene emissions, which are calculated interactively using the Model of Emissions of Gases and Aerosols from Nature (MEGAN, Guenther et al. (2006)). This simulation will be referred to as R2010 hereafter. An additional sensitivity experiment is performed (R2010_no_lu) with no anthropogenic land-use change, which is achieved by removing all vegetated tiles but the natural ones (expanding the area of the natural tiles). In both experiments, horizontal winds are nudged to those from the National Centers for Environmental Prediction reanalysis (Kalnay et al., 1996) to minimize meteorological variability between R2010 and R2010_no_lu.

For 2050, we use the vegetation, sea surface temperatures, and sea ice cover simulated by the GFDL-CM3 model under the RCP8.5 scenario in 2050 (Levy et al., 2013). RCP8.5 anthropogenic emissions for 2050 are used (Lamarque et al., 2011) except for NH_3, where we use the spatial distribution and seasonality of HTAPv2 emissions following Paulot et al. (2016). The model is run for 10 years with land-use fixed to year 2050 and we use the average of the last 9 years to minimize the impact of internal variability. This simulation will be referred to as R2050 hereafter. We perform two additional sensitivity experiments to characterize how land-use change (R2050_2010lu) and climate (R2050_2010climate) contribute to the change in deposition velocity between R2010 and R2050. The different model runs are summarized in Table 1.

Table 1. Model runs

Run ID	Climate	Land Use	Anthropogenic Emissions
R2010	2008–2010[a]	RCP8.5 (2008–2010)	HTAPv2
R2010_no_lu	2008–2010[a]	natural vegetation	HTAPv2
R2050	2050	RCP8.5 (2050)	RCP8.5 (2050)[b]
R2050_2010lu	2008–2010[a]	RCP8.5 (2008–2010)	RCP8.5 (2050)[b]
R2050_2010climate	2008–2010[a]	RCP8.5 (2050)	RCP8.5 (2050)[b]

[a] horizontal winds are nudged to NCEP

[b] with modified NH_3 emissions following Paulot et al. (2016)

3 Results and discussion

3.1 Evaluation of simulated v_d against observations

The resistance approach for calculating dry deposition velocities implemented in AM3-LM3-DD is similar to that used in most chemical transport models. However differences in implementations can result in large differences between simulated deposition velocities (Wu et al., 2018). To illustrate these differences, Fig. 2 shows the sensitivity of $v_d(SO_2)$ and $v_d(NH_3)$ to temperature, wetness, and surface acidity in three global models: MOZART (Emmons et al., 2010), GEOS-Chem (Wang et al., 1998), and AM3-LM3–DD. Under dry conditions, GEOS-Chem and AM3-LM3–DD produce identical results for $v_d(SO_2)$, with the temperature dependence driven by that of the stomatal conductance. At low and high temperatures, $v_d(NH_3)$ is faster in AM3-LM3–DD than GEOS-Chem, which reflects small differences in the assumed surface pH (6.35 and 6.6 respectively). In contrast, MOZART assumes a surface pH=5 and accounts for changes in the effective solubility of SO_2 and NH_3 with temperature, similar to Nguyen et al. (2015). The increase in solubility with decreasing temperature results in faster $v_d(X)$ at cold temperature in MOZART, while the lower pH increases $v_d(NH_3)$ and decreases $v_d(SO_2)$. The impact of surface wetness on $v_d(X)$ is only considered in MOZART and AM3-LM3 DD. In MOZART the presence of dew more than doubles $v_d(SO_2)$ but

reduces $v_d(\mathrm{NH_3})$ below 25°C. In contrast, both $v_d(\mathrm{NH_3})$ and $v_d(\mathrm{SO_2})$ increase in AM3-LM3–DD when the canopy is wet, which is supported by observations (Erisman et al., 1994, 1999; Massad et al., 2010). AM3-LM3–DD also accounts for the modulation of $R_{sf,v}(\mathrm{SO_2})$ and $R_{sf,v}(\mathrm{NH_3})$ by the acidity of the surface. Our results suggest that when $\alpha_{SN} = 2$, i.e. when the deposition of acids is twice as large as the deposition of bases, the impact of codeposition can be greater than that of canopy wetness. The large differences in the response of $v_d(\mathrm{SO_2})$ and $v_d(\mathrm{NH_3})$ to environmental conditions across three models highlight the need for detailed evaluations of $v_d(X)$ across a wide range of conditions and chemical species (Wu et al., 2018).

3.1.1 $v_d(\mathbf{SO_2})$

We first evaluate the simulated present-day (R2010) $v_d(\mathrm{SO_2})$ against a compilation of field-based $v_d(\mathrm{SO_2})$ observations (Table S3). We sample the simulated monthly diurnal cycle of $v_d(\mathrm{SO_2})$ at the location of the measurements in the tile that best represents the type of vegetation reported in the observations. We further distinguish between day-time (8am-5pm) and night-time (10pm-4am) samples and wet (wet fraction of the canopy greater than 10%) and dry periods.

Fig. 3 shows observed and simulated $v_d(\mathrm{SO_2})$ grouped among the four types of vegetation simulated by LM3 (deciduous, coniferous, tropical, and grass).

Simulated deposition velocities generally fall within a factor of 2 of the observations, with better agreement during the day than at night, when the model is biased high. This uncertainty range is similar to that reported by Wu et al. (2018) in different dry deposition models. More specifically, AM3-LM3-DD qualitatively captures the range of deposition velocities over forested ecosystems, including the slower deposition of $\mathrm{SO_2}$ in winter than in summer and under dry than under wet conditions in deciduous forests, and the fast removal of $\mathrm{SO_2}$ over coniferous forests. However, the model fails to capture the elevated $v_d(\mathrm{SO_2})$ (>1 cm/s) reported by several studies over grasslands. This may reflect uncertainties in the representation of ammonia emissions (e.g., no sub-grid heterogeneity), which could result in an underestimate of $\mathrm{SO_2}$-$\mathrm{NH_3}$ co-deposition over crops or fertilized grasslands (Nemitz et al., 2001; Flechard et al., 2013).

3.1.2 $v_d(\mathbf{HNO3, HCN, H_2O_2, OrgN})$

Fig. 4 shows the observed deposition velocities for $\mathrm{HNO_3}$, a range of organic nitrates (ISOPN, MVKN, PROPNN) derived from isoprene photooxidation (Paulot et al., 2009), HCN, and $\mathrm{H_2O_2}$. We refer the reader to Nguyen et al. (2015) for information regarding the site and Caltech observations. We compare these observations with the simulated deposition velocities at this site decomposed into its stomatal, cuticle (wet and dry), stem, and ground components.

To facilitate the comparison between simulated and observed deposition velocities, we use meteorological fields (wind speed, temperature, precipitation, and downward radiation) from the Modern-Era Retrospective Analysis for Research and Applications (MERRA) (Rienecker et al., 2011) to

9

drive a standalone version of LM3-DD. This provides a more accurate representation of the site
conditions than using meteorological fields simulated by AM3.

The compounds measured by Nguyen et al. (2015) have different chemical properties, allowing
us to evaluate the representation of different deposition pathways in AM3-LM3–DD. In particular,
HNO_3 and H_2O_2 have negligible cuticular resistance ($R_{surf,v} \simeq 0$) (Nguyen et al., 2015), such that
$v_d(X) \simeq [R_a + R_{b,v}(X)]^{-1}$ (ground deposition is negligible). Fig. 4 shows that LM3-DD captures
both $v_d(H_2O_2)$ and $v_d(HNO_3)$ well, including the faster deposition of H_2O_2 relative to HNO_3,
consistent with the dependence of R_b on $1/D_X \propto \sqrt{MW(X)}$ (equation 5). In contrast, the low
solubility and low reactivity at the leaf surface of HCN produces a large non stomatal resistance
($R_{sf,v} \ggg 1$ s/m, Nguyen et al. (2015)), such that $v_d(HCN) \simeq R_s(HCN)^{-1}$. Comparison of ob-
served and modeled $v_d(HCN)$ suggests that the Ball-Berry-Leuning model captures the stomatal
conductance well at this site. Since R_a, $R_{b,v}$, and R_s are well represented over the measurement
period, we use observations of $v_d(ISOPN)$, $v_d(MVKN)$, and $v_d(PROPNN)$ at this site to estimate
α and β for these organic nitrates (Eq. 9). We find that ($\alpha = 7$, $\beta = 1$) provide a reasonable fit for
all organic nitrates. These parameters imply that the deposition of isoprene-derived organic nitrates
is primarily controlled by dry cuticles with small contributions of stomata and stems. We note that
these parameters imply a much greater solubility and reactivity of organic nitrogen than in other
models (e.g., $\alpha = 0$, $\beta = 0.5$ in AURAMS (Zhang et al., 2002)). While we use these parameters
globally, such large differences warrant further investigations, as the deposition of organic nitrogen
may account for over 25% of the overall N deposition but remains rarely measured (Jickells et al.,
2013).

Finally, we note that the comparison against SOAS observations points to a significant high bias in
simulated night-time deposition velocity. Since this bias is found for all species including H_2O_2 and
HNO_3, this suggests that the model underestimates the aerodynamic resistance (R_a) during these
periods.

3.2 Impact of land heterogeneities on present-day N deposition

Fig. 5 shows the simulated dry deposition of oxidized N (dominated by HNO_3) and reduced N
(dominated by NH_3) as well as the total N deposition (wet+dry) in North America. As noted in
previous studies (Zhang et al., 2012; Lamarque et al., 2013), the overall pattern of N deposition
mirrors the underlying distribution of NH_3 and NO emissions, with high deposition in the Northeast
and greater contribution of reduced nitrogen to N deposition in the US Midwest and North Carolina
than elsewhere in the Eastern US.

The simulated dry deposition represents the sum of the deposition fluxes to the tiles that comprise
each grid cell. Fig. 5 (middle column) shows that N deposition over natural vegetation is generally
greater than the grid-cell average, which is consistent with faster deposition velocities over forests
relative to grasslands (Finkelstein (2001); Hicks (2006) and Fig. S1). Overall, the simulated total

310 N deposition to natural ecosystems exceeds the grid-box average deposition by 10 to 30% over most of the Eastern and Central US. This enhancement is largest in regions where land-use change has caused a large decrease in vegetation height and LAI (e.g., in the US Midwest and Northeast, Fig. S2) and smallest in regions with little agricultural activity (e.g., most of Canada) or where managed vegetation differs little in height and LAI from natural vegetation (e.g., in the Western

315 US, Fig. S2). Fig. 5 (middle column) also shows that the dry deposition of NH_x exhibits a greater enhancement over natural vegetation than the dry deposition of NO_y, consistent with the greater sensitivity of $v_d(NH_3)$ than $v_d(HNO_3)$ to surface properties (Fig. S3). The enhancements of the dry deposition of NH_x over natural vegetation is likely to be underestimated in AM3-LM3-DD as the surface bidirectional exchange of NH_3 tends to reduce its deposition in source regions.

320 Fig. 5 (right column) also shows that water bodies receive more reduced N but less oxidized N through dry deposition than the grid-box average. These differences can be attributed to the large effective solubility of NH_3 in freshwater, which results in lower $R_{sf,g}(NH_3)$ than over vegetated surfaces ($R_{sf,g}(HNO_3)$ is low over all surfaces). Our model suggests that $v_d(HNO_3)$ is generally slower over water bodies than over vegetated surfaces because of the lower roughness height of

325 water bodies (see Fig. S3). The westward increase in the ratio of NH_3 to NO emissions thus results in water bodies receiving less N than the average grid cell in the Eastern US and Canada but more in the Central and Western US. .

3.3 Impact of anthropogenic land-use change on present-day N deposition

Fig. 6 shows the change in dry NO_y, dry NH_x, and total N deposition associated with anthropogenic

330 land-use change, which is estimated by comparing R2010 and R2010_no_lu. We find that anthropogenic land-use change reduces dry NO_y, dry NH_x, and total N deposition over the contiguous US by 8%, 26%, and 6%, respectively. The reduction in N deposition associated with anthropogenic land-use change is largest in the Central and Eastern US, where deforestation has caused a large reduction in LAI and vegetation height (Fig. S2).

335 While anthropogenic land use is estimated to reduce the overall N deposition in the contiguous US, we find that it tends to increase the surface concentration of reactive nitrogen species, which leads to greater N deposition on the remaining natural vegetation. Fig. 6 shows that land use has important implications for N deposition at national parks, which are best represented by natural vegetation tiles. For instance, we find that anthropogenic land-use change is associated with a 14%

340 reduction in the overall N deposition in the region of Shenandoah National Park, but an increase of 9% on natural vegetation in the same grid box. The slower removal of N near source regions also facilitates N export to remote regions, such as Eastern Canada, where N deposition (primarily through wet deposition) increases by more than 10%. This suggests that anthropogenic land-use change in North America has contributed to the increase of N deposition to natural ecosystems both

345 near source regions and in remote receptor regions.

3.4 Implications for future N deposition

Fig. 7 shows the simulated difference between N deposition in 2008–2010 (R2010) and 2050 (R2050). This difference reflects changes in anthropogenic emissions as well as changes in climate and land properties induced by climate and land-use change. Total N deposition is projected to increase by 9% over the contiguous US. Most of the increase is driven by greater deposition in the Midwest and Western US associated with higher NH_3 emissions (+40%). In contrast, N deposition is projected to decrease in the Eastern US following the decrease of NO emissions (-47%, mostly in the Eastern US).

We find a small increase (<10%) in the deposition velocity of HNO_3 over most of the US between R2010 and R2050 (Fig. S4). This is attributed to a reduction in the land fraction devoted to agriculture in RCP8.5 between 2010 and 2050 (Davies-Barnard et al., 2014), which results in taller vegetation and higher LAI. The impact of this change in land use between 2010 and 2050 is larger for $v_d(NH_3)$, which increases by more >10% over most of the Midwest and Eastern US. However, in the Eastern and Midwest US, this increase is more than compensated by a reduction in acid deposition, which results in an overall decrease of $v_d(NH_3)$ of 10 to 20% over most of the Eastern US. This highlights the need to better characterize the impact of the co-deposition of acids and ammonia on the removal of ammonia to improve projection of future N deposition.

Fig. 7 also shows that trends in N deposition simulated for all land types tend to be amplified over natural vegetation, because of the faster deposition velocities as discussed earlier. In contrast, water bodies are projected to experience an increase in N deposition over most of the US, including in regions which experience an overall decrease in N deposition. This contrast is driven by the faster removal of NH_3 over water relative to managed vegetation, which result in greater sensitivity to changes in the emissions of reduced N. The different responses of N deposition on natural tiles and water tiles are important for projections of N deposition in national parks, where N deposition to both vegetation and water bodies is of concern. For instance, the changes in N deposition to natural vegetation from 2010 to 2050 at Voyageurs and Shenandoah national parks are 30% greater than simulated in the grid box where they are located, while N deposition to water bodies in the Shenandoah region is projected to increase by 16%, even though overall N deposition for the grid decreases by 18% in this region.

4 Conclusions

Our study highlights the importance of accounting for surface heterogeneities and anthropogenic land use in modulating the magnitude and trend of N deposition. Here, we leverage the tiled structure of the GFDL land model to efficiently represent the sub-grid scale heterogeneity of surface properties and their evolution in a changing climate. We have shown that the shift of N emissions from oxidized to reduced N in North America will exacerbate the sensitivity of N deposition to

small-scale heterogeneities, which highlights the need to improve the representation of non-stomatal surface resistances ($R_{sf,v}$, $R_{sf,s}$, and $R_{sf,g}$) including their modulation by canopy wetness and acidity (Flechard et al., 2013; Wentworth et al., 2016; Wu et al., 2018).

385 Our approach is best suited to long time scales (decadal to centennial) and is complementary to ongoing efforts to improve the representation of present-day N deposition using a combination of high-resolution models and observations (Schwede and Lear, 2014). Future work will aim at coupling the representation of dry deposition presented here to the N cycle in the GFDL land model (Gerber et al., 2010), which will enable us to represent the bidirectional exchange of NH_3 (Nemitz et al., 2001; Flechard et al., 2013; Bash et al., 2013) and improve our understanding of the impact

390 of N deposition on ecosystems and carbon cycling (Magnani et al., 2007; Janssens et al., 2010; Fleischer et al., 2013, 2015).

395
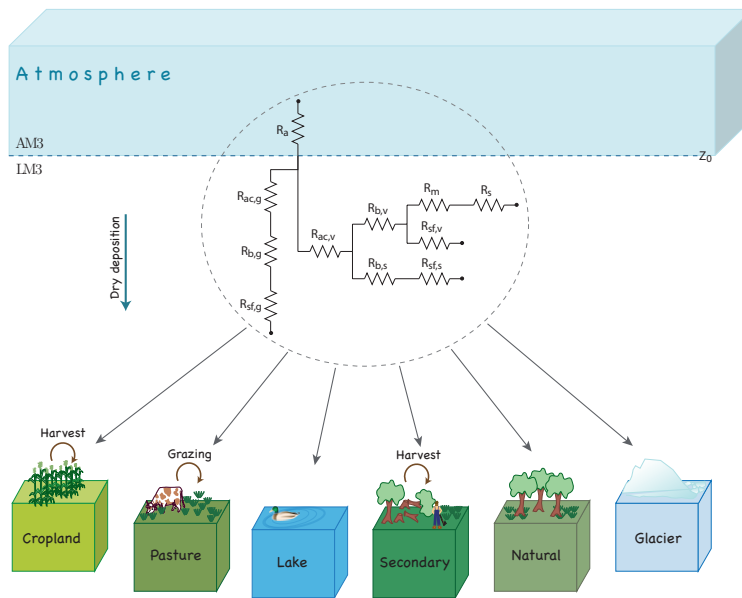
Figure 1. Schematic representation of the resistance scheme used to represent the dry deposition of gaseous tracers for each tile. R_a, $R_{b,i}$, R_{ac}, R_m , R_s, and $R_{sf,i}$ are the aerodynamic resistance, laminar resistance, canopy aerodynamic resistance, mesophyl resistance, stomatal resistance, and surface resistance, respectively. The g, s, and v indexes (i) refer to ground, stem, and vegetation. Note that for clarity deposition on soil and vegetation that are covered by snow or liquid water are not shown.
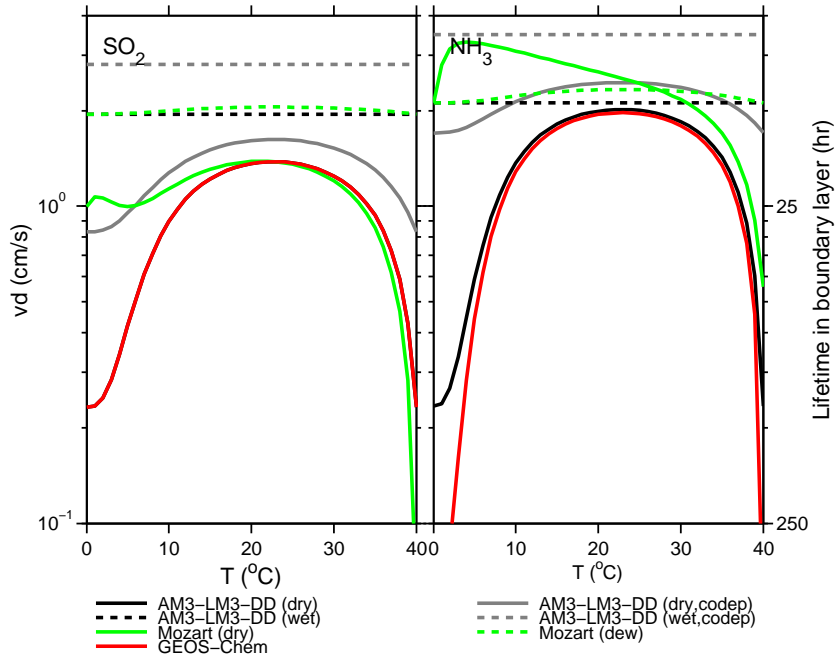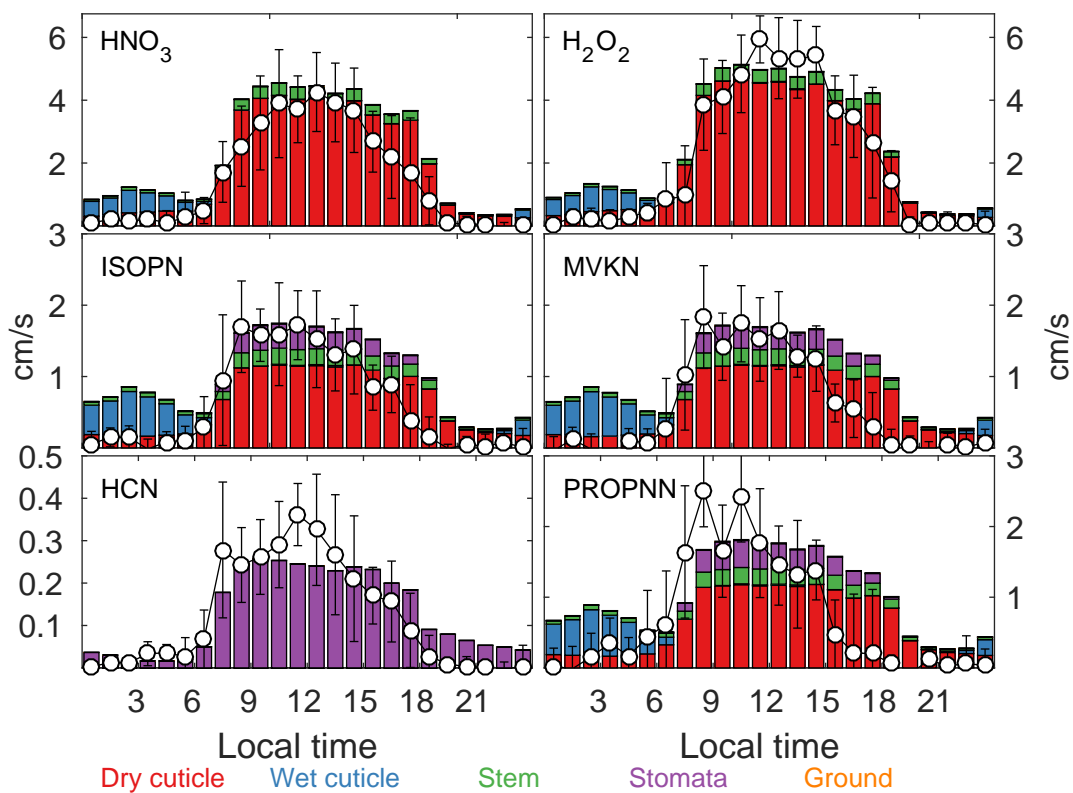
Figure 2. Simulated deposition velocity of NH_3 and SO_2 over a coniferous forest (LAI=5, $u_\star = 0.5$m/s, RH=80%) at different canopy wetness and temperature. To facilitate comparison across models, we use the same $R_a = 20$s/m, R_b (Hicks et al., 1987) and R_s (Wesely, 1989) for all models. Solar irradiation increases linearly from 0 to 800 W/m^2 with temperature. We neglect deposition to the ground and stems. Co-dep refers to the decrease in $R_{sf,v}(SO_2)$ and $R_{sf,v}(NH_3)$ associated with base and acid deposition respectively. For illustrative purposes, the ratio of acid to base deposition is set to 0.5 for SO_2 and 2 for NH_3. The lifetimes of SO_2 and NH_3 are estimated assuming a boundary layer height of 900m. GEOS-Chem and AM3-LM3–DD produce identical results for SO_2 under dry conditions.
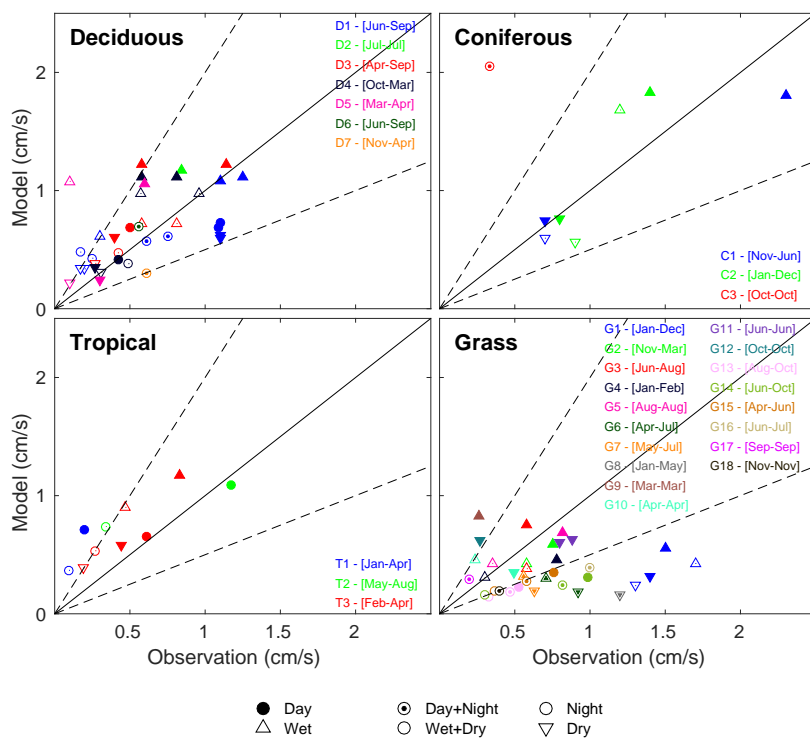
Figure 3. Observed and simulated deposition velocities of SO$_2$ for different vegetation types. The symbol shape indicates the canopy status: wet (upward pointing triangle), dry (downward point triangle), circle (average). The symbol fill indicates the time period: filled (day), half-filled (day+night), empty (night). The monthly diurnal cycle of deposition velocities simulated by AM3-LM3-DD (R2010 simulation) is sampled at each observation site in the tile that best represents the observed ecosystem accounting for the month, time of day and canopy wetness status when the observations were collected . References for the different sites are given in Table S3.

Figure 4. Observed (circles +/- standard deviation) and simulated (bars) dry deposition velocities for several nitrogen–containing species and hydrogen peroxide over the Talladega National Forest (Southeast US) in June 2013 (5 days, Nguyen et al. (2015)). The bar colors indicate the contribution of the different surfaces to the overall surface removal of the chemical tracer.
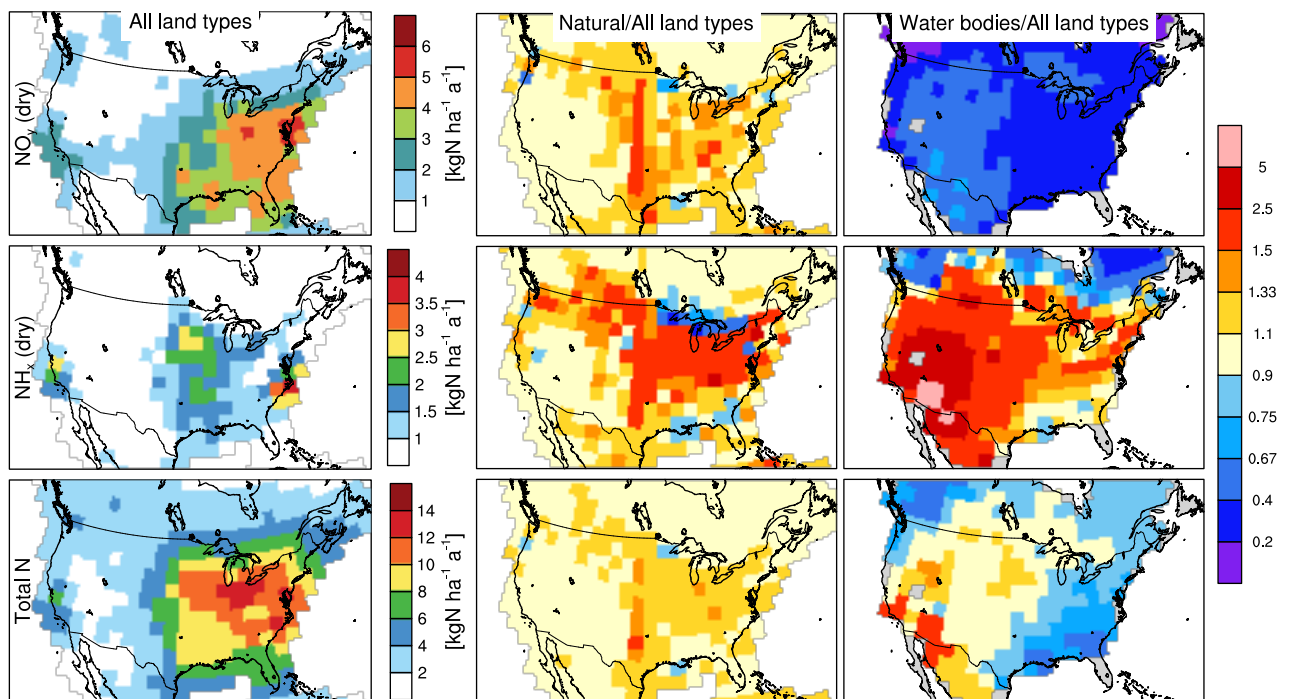
Figure 5. Simulated reactive nitrogen deposition (left column) from dry oxidized nitrogen deposition (first row), dry reduced nitrogen deposition (second row), and total nitrogen deposition (bottom row) over the 2008–2010 period. The ratio between the deposition on selected land types and the grid cell average deposition is shown in the middle (for natural vegetation) and right columns (water bodies)
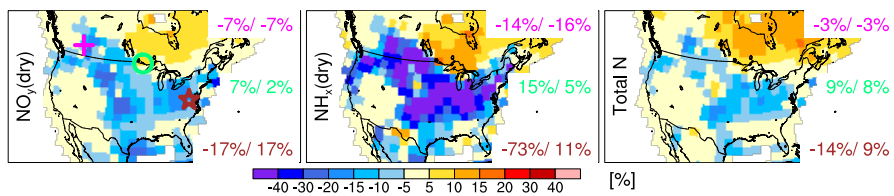
Figure 6. Relative change in the 2008–2010 average land deposition of dry oxidized nitrogen (left), dry reduced nitrogen (center), and total nitrogen (right) associated with anthropogenic land-use change. The relative change is shown as (with land-use - without land land-use)/with land-use. From top right to bottom right, the percentages indicate the change in N deposition at Banff National Park (cross), Voyageurs National Park (circle), and Shenandoah National Park (star) at the grid box level and on natural vegetation, a better proxy for these parks.
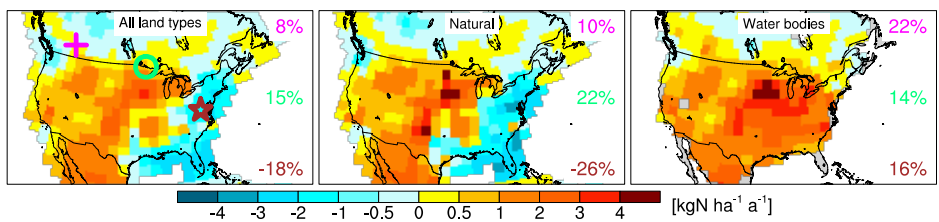
Figure 7. Simulated change in reactive nitrogen deposition from 2010 to 2050 in the RCP8.5 scenario at the grid box level (left), on natural tiles (center) and on water bodies (right). From top right to bottom right, the percentages indicate the change in N deposition at Banff National Park (cross), Voyageurs National Park (circle), and Shenandoah National Park (star) at the grid box level and on natural vegetation tiles respectively. The fractional change in N deposition over the contiguous US is indicated in inset (bottom left).

References

Baron, J. S., Hall, E. K., Nolan, B. T., Finlay, J. C., Bernhardt, E. S., Harrison, J. A., Chan, F., and Boyer, E. W.: The interactive effects of excess reactive nitrogen and climate change on aquatic ecosystems and water resources of the United States, Biogeochemistry, pp. 1–22, 2012.

Bash, J. O., Cooter, E. J., Dennis, R. L., Walker, J. T., and Pleim, J. E.: Evaluation of a regional air-quality model with bidirectional NH_3 exchange coupled to an agroecosystem model, Biogeosciences, 10, 1635–1645, 2013.

Bobbink, R., Hicks, K., Galloway, J., Spranger, T., Alkemade, R., Ashmore, M., Bustamante, M., Cinderby, S., Davidson, E., Dentener, F., Emmett, B., Erisman, J.-W., Fenn, M., Gilliam, F., Nordin, A., Pardo, L., and De Vries, W.: Global assessment of nitrogen deposition effects on terrestrial plant diversity: a synthesis, Ecol. Appl., 20, 30–59, 2010.

Bonan, G. B.: Land surface model (LSM version 1.0) for ecological, hydrological, and atmospheric studies: Technical description and users guide. Technical note, Tech. rep., National Center for Atmospheric Research, Boulder, CO (United States). Climate and Global Dynamics Div., 1996.

Bondeau, A., Smith, P., Zaehle, S., Schaphoff, S., Lucht, W., Cramer, W., Gerten, D., Lotze-Campen, H., Müller, C., Reichstein, M., et al.: Modelling the role of agriculture for the 20th century global terrestrial carbon balance, Global Change Biol., 13, 679–706, 2007.

Bytnerowicz, A., Johnson, R., Zhang, L., Jenerette, G., Fenn, M., Schilling, S., and Gonzalez-Fernandez, I.: An empirical inferential method of estimating nitrogen deposition to Mediterranean-type ecosystems: the San Bernardino Mountains case study, Environmental Pollution, 203, 69–88, doi:10.1016/j.envpol.2015.03.028, https://doi.org/10.1016/j.envpol.2015.03.028, 2015.

Choudhury, B. J. and Monteith, J. L.: A four-layer model for the heat budget of homogeneous land surfaces, Quarterly Journal of the Royal Meteorological Society, 114, 373–398, doi:10.1002/qj.49711448006, https://doi.org/10.1002/qj.49711448006, 1988.

Davies-Barnard, T., Valdes, P. J., Singarayer, J. S., Pacifico, F. M., and Jones, C. D.: Full effects of land use change in the representative concentration pathways, Environ. Res. Lett., 9, 114 014, doi:10.1088/1748-9326/9/11/114014, http://stacks.iop.org/1748-9326/9/i=11/a=114014, 2014.

De Schrijver, A., Staelens, J., Wuyts, K., Van Hoydonck, G., Janssen, N., Mertens, J., Gielis, L., Geudens, G., Augusto, L., and Verheyen, K.: Effect of vegetation type on throughfall deposition and seepage flux, Environ. Pollut., 153, 295–303, 2008.

de Vries, W., Hettelingh, J.-P., and Posch, M., eds.: Critical Loads and Dynamic Risk Assessments, vol. 25 of *Environmental Pollution*, Springer Netherlands, Dordrecht, 2015.

Dentener, F., Drevet, J., Lamarque, J. F., Bey, I., Eickhout, B., Fiore, A. M., Hauglustaine, D., Horowitz, L. W., Krol, M., Kulshrestha, U. C., Lawrence, M., Galy-Lacaux, C., Rast, S., Shindell, D., Stevenson, D., Van Noije, T., Atherton, C., Bell, N., Bergman, D., Butler, T., Cofala, J., Collins, B., Doherty, R., Ellingsen, K., Galloway, J., Gauss, M., Montanaro, V., Müller, J. F., Pitari, G., Rodriguez, J., Sanderson, M., Solmon, F., Strahan, S., Schultz, M., Sudo, K., Szopa, S., and Wild, O.: Nitrogen and sulfur deposition on regional and global scales: A multimodel evaluation, Global Biogeochem. Cycles, 20, B4003, 2006.

Devaraju, N., Bala, G., Caldeira, K., and Nemani, R.: A model based investigation of the relative importance of CO_2-fertilization, climate warming, nitrogen deposition and land use change on the global terrestrial carbon uptake in the historical period, Clim. Dyn., pp. 1–18, 2015.

Dezi, S., Medlyn, B. E., Tonon, G., and Magnani, F.: The effect of nitrogen deposition on forest carbon sequestration: a model-based analysis, Glob. Chang. Biol., 16, 1470–1486, 2010.

Dirnböck, T., Foldal, C., Djukic, I., Kobler, J., Haas, E., Kiese, R., and Kitzler, B.: Historic nitrogen deposition determines future climate change effects on nitrogen retention in temperate forests, Climatic Change, 144, 221–235, doi:10.1007/s10584-017-2024-y, https://doi.org/10.1007/s10584-017-2024-y, 2017.

Dise, N. B.: The European Nitrogen Assessment: Sources, Effects and Policy Perspectives, chap. 20, Cambridge University Press, 2011.

Donner, L. J., Wyman, B. L., Hemler, R. S., Horowitz, L. W., Ming, Y., Zhao, M., Golaz, J.-C., Ginoux, P., Lin, S.-J., Schwarzkopf, M. D., Austin, J., Alaka, G., Cooke, W. F., Delworth, T. L., Freidenreich, S. M., Gordon, C. T., Griffies, S. M., Held, I. M., Hurlin, W. J., Klein, S. A., Knutson, T. R., Langenhorst, A. R., Lee, H.-C., Lin, Y., Magi, B. I., Malyshev, S. L., Milly, P. C. D., Naik, V., Nath, M. J., Pincus, R., Ploshay, J. J., Ramaswamy, V., Seman, C. J., Shevliakova, E., Sirutis, J. J., Stern, W. F., Stouffer, R. J., Wilson, R. J., Winton, M., Wittenberg, A. T., and Zeng, F.: The Dynamical Core, Physical Parameterizations, and Basic Simulation Characteristics of the Atmospheric Component AM3 of the GFDL Global Coupled Model CM3, J. Clim., 24, 3484–3519, 2011.

Dore, A., Vieno, M., Tang, Y., Dragosits, U., Dosio, A., Weston, K., and Sutton, M.: Modelling the atmospheric transport and deposition of sulphur and nitrogen over the United Kingdom and assessment of the influence of SO2 emissions from international shipping, Atmospheric Environment, 41, 2355–2367, doi:10.1016/j.atmosenv.2006.11.013, https://doi.org/10.1016/j.atmosenv.2006.11.013, 2007.

Dore, A. J., Kryza, M., Hall, J. R., Hallsworth, S., Keller, V. J. D., Vieno, M., and Sutton, M. A.: The influence of model grid resolution on estimation of national scale nitrogen deposition and exceedance of critical loads, Biogeosciences, 9, 1597–1609, doi:10.5194/bg-9-1597-2012, https://doi.org/10.5194/bg-9-1597-2012, 2012.

Ellis, R. A., Jacob, D. J., Sulprizio, M. P., Zhang, L., Holmes, C. D., Schichtel, B. A., Blett, T., Porter, E., Pardo, L. H., and Lynch, J. A.: Present and future nitrogen deposition to national parks in the United States: critical load exceedances, Atmos. Chem. Phys., 13, 9083–9095, 2013.

Emmons, L. K., Walters, S., Hess, P. G., Lamarque, J.-F., Pfister, G. G., Fillmore, D., Granier, C., Guenther, A., Kinnison, D., Laepple, T., Orlando, J., Tie, X., Tyndall, G., Wiedinmyer, C., Baughcum, S. L., and Kloster, S.: Description and evaluation of the Model for Ozone and Related chemical Tracers, version 4 (MOZART-4), Geosci. Model Dev., 3, 43–67, 2010.

Erisman, J. W.: Evaluation of a surface resistance parametrization of sulphur dioxide, Atmos. Environ., 28, 2583–2594, 1994.

Erisman, J. W., Pul, A. V., and Wyers, P.: Parametrization of surface resistance for the quantification of atmospheric deposition of acidifying pollutants and ozone, Atmos. Environ., 28, 2595 – 2607, doi:http://dx.doi.org/10.1016/1352-2310(94)90433-2, http://www.sciencedirect.com/science/article/pii/1352231094904332, 1994.

Erisman, J. W., Hogenkamp, J. E. M., Putten, E. M. v., Uiterwijk, J. W., Kemkers, E., Wiese, C. J., and Mennen, M. G.: Long-term Continuous Measurements of SO$_2$ Dry Deposition over the Speulder Forest, Water. Air. Soil Pollut., 109, 237–262, doi:10.1023/A:1005097722854, http://link.springer.com/article/10.1023/A%3A1005097722854, 1999.

22

Erisman, J. W., Galloway, J. N., Seitzinger, S., Bleeker, A., Dise, N. B., Petrescu, A. M. R., Leach, A. M., and Vries, W. d.: Consequences of human modification of the global nitrogen cycle, Phil. Trans. R. Soc. B, 368, 20130116, 2013.

480   Finkelstein, P. L.: Deposition Velocities of SO_2 and O_3 over Agricultural and Forest Ecosystems, Water, Air and Soil Pollution: Focus, 1, 49–57, 2001.

Flechard, C. R., Massad, R.-S., Loubet, B., Personne, E., Simpson, D., Bash, J. O., Cooter, E. J., Nemitz, E., and Sutton, M. A.: Advances in understanding, models and parameterizations of biosphere-atmosphere ammonia exchange, Biogeosciences, 10, 5183–5225, 2013.

485   Fleischer, K., Rebel, K. T., van der Molen, M. K., Erisman, J. W., Wassen, M. J., van Loon, E. E., Montagnani, L., Gough, C. M., Herbst, M., Janssens, I. A., Gianelle, D., and Dolman, A. J.: The contribution of nitrogen deposition to the photosynthetic capacity of forests, Global Biogeochem. Cycles, 27, 187–199, 2013.

Fleischer, K., Wårlind, D., van der Molen, M. K., Rebel, K. T., Arneth, A., Erisman, J. W., Wassen, M. J., Smith, B., Gough, C. M., Margolis, H. A., Cescatti, A., Montagnani, L., Arain, A., and Dolman, A. J.: Low

490   historical nitrogen deposition effect on carbon sequestration in the boreal zone, J. Geophys. Res. Biogeosci., 120, 2015JG002988, 2015.

Fowler, D., Coyle, M., Skiba, U., Sutton, M. A., Cape, J. N., Reis, S., Sheppard, L. J., Jenkins, A., Grizzetti, B., Galloway, J. N., Vitousek, P., Leach, A., Bouwman, A. F., Butterbach-Bahl, K., Dentener, F., Stevenson, D., Amann, M., and Voss, M.: The global nitrogen cycle in the twenty-first century, Philos. Trans. R. Soc.

495   London, Ser. B, 368, 2013.

Gerber, S., Hedin, L. O., Oppenheimer, M., Pacala, S. W., and Shevliakova, E.: Nitrogen cycling and feedbacks in a global dynamic land model, Global Biogeochem. Cycles, 24, GB1001, 2010.

Grizzetti, B.: The European Nitrogen Assessment: Sources, Effects and Policy Perspectives, chap. 17, Cambridge University Press, 2011.

500   Guenther, A., Karl, T., Harley, P., Wiedinmyer, C., Palmer, P. I., and Geron, C.: Estimates of global terrestrial isoprene emissions using MEGAN (Model of Emissions of Gases and Aerosols from Nature), Atmos. Chem. Phys., 6, 3181–3210, 2006.

Gundale, M. J., From, F., Bach, L. H., and Nordin, A.: Anthropogenic nitrogen deposition in boreal forests has a minor impact on the global carbon cycle, Glob. Chang. Biol., 20, 276–286, 2014.

505   Hertel, O.: The European Nitrogen Assessment: Sources, Effects and Policy Perspectives, chap. 14, Cambridge University Press, 2011.

Hicks, B. B.: Dry deposition to forests—On the use of data from clearings, Agric. For. Meteorol., 136, 214–221, doi:10.1016/j.agrformet.2004.06.013, http://www.sciencedirect.com/science/article/pii/S0168192305002066, 2006.

510   Hicks, B. B.: On Estimating Dry Deposition Rates in Complex Terrain, Journal of Applied Meteorology and Climatology, 47, 1651–1658, 2008.

Hicks, B. B., Baldocchi, D. D., Meyers, T. P., Hosker, R. P., and Matt, D. R.: A preliminary multiple resistance routine for deriving dry deposition velocities from measured quantities, Water, Air, & Soil Pollution, 36, 311–330, 1987.

515   Högberg, P.: What is the quantitative relation between nitrogen deposition and forest carbon sequestration?, Glob. Chang. Biol., 18, 1–2, 2012.

Huang, L., McDonald-Buller, E. C., McGaughey, G., Kimura, Y., and Allen, D. T.: The impact of drought on ozone dry deposition over eastern Texas, Atmos. Environ., 127, 176–186, doi:10.1016/j.atmosenv.2015.12.022, http://www.sciencedirect.com/science/article/pii/S1352231015305902, 2016.

Hurtt, G. C., Chini, L. P., Frolking, S., Betts, R. A., Feddema, J., Fischer, G., Fisk, J. P., Hibbard, K., Houghton, R. A., Janetos, A., Jones, C. D., Kindermann, G., Kinoshita, T., Goldewijk, K. K., Riahi, K., Shevliakova, E., Smith, S., Stehfest, E., Thomson, A., Thornton, P., Vuuren, D. P. v., and Wang, Y. P.: Harmonization of land-use scenarios for the period 1500–2100: 600 years of global gridded annual land-use transitions, wood harvest, and resulting secondary lands, Clim. Change, 109, 117–161, 2011.

Janssens, I. A., Dieleman, W., Luyssaert, S., Subke, J.-A., Reichstein, M., Ceulemans, R., Ciais, P., Dolman, A. J., Grace, J., Matteucci, G., Papale, D., Piao, S. L., Schulze, E.-D., Tang, J., and Law, B.: Reduction of forest soil respiration in response to nitrogen deposition, Nature Geosci, 3, 315–322, 2010.

Janssens-Maenhout, G., Crippa, M., Guizzardi, D., Dentener, F., Muntean, M., Pouliot, G., Keating, T., Zhang, Q., Kurokawa, J., Wankmüller, R., Denier van der Gon, H., Kuenen, J. J. P., Klimont, Z., Frost, G., Darras, S., Koffi, B., and Li, M.: HTAP_v2.2: a mosaic of regional and global emission grid maps for 2008 and 2010 to study hemispheric transport of air pollution, Atmos. Chem. Phys., 15, 11 411–11 432, doi:10.5194/acp-15-11411-2015, http://www.atmos-chem-phys.net/15/11411/2015/, 2015.

Jensen, N. O. and Hummelshøj, P.: Derivation of canopy resistance for water vapour fluxes over a spruce forest, using a new technique for the viscous sublayer resistance, Agric. For. Meteorol., 73, 339–352, 1995.

Jensen, N. O. and Hummelshøj, P.: Erratum, Agric. For. Meteorol., 85, 289, doi:10.1016/S0168-1923(97)00024-5, http://www.sciencedirect.com/science/article/pii/S0168192397000245, 1997.

Jickells, T., Baker, A. R., Cape, J. N., Cornell, S. E., and Nemitz, E.: The cycling of organic nitrogen through the atmosphere, Philos. Trans. R. Soc. London, Ser. B, 368, PMID: 23713115, 2013.

Johansson, O., Palmqvist, K., and Olofsson, J.: Nitrogen deposition drives lichen community changes through differential species responses, Glob. Chang. Biol., 18, 2626–2635, 2012.

Kalnay, E., Kanamitsu, M., Kistler, R., Collins, W., Deaven, D., Gandin, L., Iredell, M., Saha, S., White, G., Woollen, J., Zhu, Y., Leetmaa, A., Reynolds, R., Chelliah, M., Ebisuzaki, W., Higgins, W., Janowiak, J., Mo, K. C., Ropelewski, C., Wang, J., Jenne, R., and Joseph, D.: The NCEP/NCAR 40-Year Reanalysis Project, Bull. Am. Meteorol. Soc., 77, 437–471, 1996.

Lamarque, J.-F., Kyle, G., Meinshausen, M., Riahi, K., Smith, S., van Vuuren, D., Conley, A., and Vitt, F.: Global and regional evolution of short-lived radiatively-active gases and aerosols in the Representative Concentration Pathways, Clim. Change, 109, 191–212, 10.1007/s10584-011-0155-0, 2011.

Lamarque, J.-F., Dentener, F., McConnell, J., Ro, C.-U., Shaw, M., Vet, R., Bergmann, D., Cameron-Smith, P., Dalsoren, S., Doherty, R., Faluvegi, G., Ghan, S. J., Josse, B., Lee, Y. H., MacKenzie, I. A., Plummer, D., Shindell, D. T., Skeie, R. B., Stevenson, D. S., Strode, S., Zeng, G., Curran, M., Dahl-Jensen, D., Das, S., Fritzsche, D., and Nolan, M.: Multi-model mean nitrogen and sulfur deposition from the Atmospheric Chemistry and Climate Model Intercomparison Project (ACCMIP): evaluation of historical and projected future changes, Atmos. Chem. Phys., 13, 7997–8018, 2013.

555   Lepori, F. and Keck, F.: Effects of Atmospheric Nitrogen Deposition on Remote Freshwater Ecosystems, Ambio, 41, 235–246, doi:10.1007/s13280-012-0250-0, http://www.ncbi.nlm.nih.gov/pmc/articles/PMC3357855/, 2012.

Leuning, R.: A critical appraisal of a combined stomatal-photosynthesis model for C3 plants, Plant, Cell & Environment, 18, 339–355, 1995.

560   Levy, H., Horowitz, L. W., Schwarzkopf, M. D., Ming, Y., Golaz, J.-C., Naik, V., and Ramaswamy, V.: The roles of aerosol direct and indirect effects in past and future climate change, J. Geophys. Res. Atmos., 118, 4521–4532, 2013.

Li, Y., Schichtel, B. A., Walker, J. T., Schwede, D. B., Chen, X., Lehmann, C. M. B., Puchalski, M. A., Gay, D. A., and Collett, J. L.: Increasing importance of deposition of reduced nitrogen in the United States, Proc.
565   Natl. Acad. Sci. U.S.A., p. 201525736, doi:10.1073/pnas.1525736113, http://www.pnas.org/content/early/2016/05/04/1525736113, 2016.

Loubet, B., Cellier, P., Milford, C., and Sutton, M. A.: A coupled dispersion and exchange model for short-range dry deposition of atmospheric ammonia, Quart. J. Roy. Meteor. Soc., 132, 1733–1763, 2006.

Magnani, F., Mencuccini, M., Borghetti, M., Berbigier, P., Berninger, F., Delzon, S., Grelle, A., Hari, P., Jarvis,
570   P. G., Kolari, P., Kowalski, A. S., Lankreijer, H., Law, B. E., Lindroth, A., Loustau, D., Manca, G., Moncrieff, J. B., Rayment, M., Tedeschi, V., Valentini, R., and Grace, J.: The human footprint in the carbon cycle of temperate and boreal forests, Nature, 447, 849–851, 2007.

Malm, W. C., Rodriguez, M. A., Schichtel, B. A., Gebhart, K. A., Thompson, T. M., Barna, M. G., Benedict, K. B., Carrico, C. M., and Collett Jr., J. L.: A hybrid modeling ap-
575   proach for estimating reactive nitrogen deposition in Rocky Mountain National Park, Atmos. Environ., 126, 258–273, doi:10.1016/j.atmosenv.2015.11.060, http://www.sciencedirect.com/science/article/pii/S1352231015305677, 2016.

Malyshev, S., Shevliakova, E., Stouffer, R. J., and Pacala, S. W.: Contrasting Local versus Regional Effects of Land-Use-Change-Induced Heterogeneity on Historical Climate: Analysis with the GFDL Earth System
580   Model, J. Clim., 28, 5448–5469, 2015.

Massad, R.-S., Nemitz, E., and Sutton, M. A.: Review and parameterisation of bi-directional ammonia exchange between vegetation and the atmosphere, Atmos. Chem. Phys., 10, 10 359–10 386, 2010.

Meunier, C. L., Gundale, M. J., Sánchez, I. S., and Liess, A.: Impact of nitrogen deposition on forest and lake food webs in nitrogen-limited environments, Glob. Chang. Biol., 22, 164–179, doi:10.1111/gcb.12967,
585   http://onlinelibrary.wiley.com/doi/10.1111/gcb.12967/abstract, 2016.

Milly, P. C. D., Malyshev, S. L., Shevliakova, E., Dunne, K. A., Findell, K. L., Gleeson, T., Liang, Z., Phillipps, P., Stouffer, R. J., and Swenson, S.: An Enhanced Model of Land Water and Energy for Global Hydrologic and Earth-System Studies, J. Hydrometeorol., 15, 1739–1761, 2014.

Naik, V., Horowitz, L. W., Fiore, A. M., Ginoux, P., Mao, J., Aghedo, A. M., and Levy, H.: Impact of prein-
590   dustrial to present-day changes in short-lived pollutant emissions on atmospheric composition and climate forcing, J. Geophys. Res. Atmos., 118, 8086–8110, 2013.

Neirynck, J., Flechard, C. R., and Fowler, D.: Long-term (13 years) measurements of SO_2 fluxes over a forest and their control by surface chemistry, Agric. For. Meteorol., 151, 1768–1780, 2011.

Nemitz, E., Milford, C., and Sutton, M. A.: A two-layer canopy compensation point model for describing bi-
directional biosphere-atmosphere exchange of ammonia, Quart. J. Roy. Meteor. Soc., 127, 815–833, 2001.

Nguyen, T. B., Crounse, J. D., Teng, A. P., Clair, J. M. S., Paulot, F., Wolfe, G. M., and Wennberg, P. O.:
Rapid deposition of oxidized biogenic compounds to a temperate forest, Proc. Natl. Acad. Sci. U.S.A., 112,
E392–E401, doi:10.1073/pnas.1418702112, http://www.pnas.org/content/112/5/E392, 2015.

Ochoa-Hueso, R., Allen, E. B., Branquinho, C., Cruz, C., Dias, T., Fen, M. E., Manrique, E., Pérez-Corona,
M. E., Sheppard, L. J., and Stock, W. D.: Nitrogen deposition effects on Mediterranean-type ecosystems: An
ecological assessment, Environ. Pollut., 159, 2265 – 2279, 2011.

Pardo, L. H., Fenn, M. E., Goodale, C. L., Geiser, L. H., Driscoll, C. T., Allen, E. B., Baron, J. S., Bobbink,
R., Bowman, W. D., Clark, C. M., Emmett, B., Gilliam, F. S., Greaver, T. L., Hall, S. J., Lilleskov, E. A.,
Liu, L., Lynch, J. A., Nadelhoffer, K. J., Perakis, S. S., Robin-Abbott, M. J., Stoddard, J. L., Weathers, K. C.,
and Dennis, R. L.: Effects of nitrogen deposition and empirical nitrogen critical loads for ecoregions of the
United States, Ecol. Appl., 21, 3049–3082, 2011.

Paulot, F., Crounse, J. D., Kjaergaard, H. G., Kroll, J. H., Seinfeld, J. H., and Wennberg, P. O.: Isoprene photoox-
idation: new insights into the production of acids and organic nitrates, Atmos. Chem. Phys., 9, 1479–1501,
2009.

Paulot, F., Jacob, D. J., and Henze, D. K.: Sources and Processes Contributing to Nitrogen Deposition: An
Adjoint Model Analysis Applied to Biodiversity Hotspots Worldwide, Environ. Sci. Technol., 47, 3226–
3233, 2013.

Paulot, F., Jacob, D. J., Pinder, R. W., Bash, J. O., Travis, K., and Henze, D. K.: Ammonia emissions in the
United States, European Union, and China derived by high-resolution inversion of ammonium wet deposition
data: Interpretation with a new agricultural emissions inventory (MASAGE_NH3), J. Geophys. Res. Atmos.,
119, 4343–4364, 2014.

Paulot, F., Ginoux, P., Cooke, W. F., Donner, L. J., Fan, S., Lin, M.-Y., Mao, J., Naik, V., and Horowitz, L. W.:
Sensitivity of nitrate aerosols to ammonia emissions and to nitrate chemistry: implications for present and
future nitrate optical depth, Atmos. Chem. Phys., 16, 1459–1477, doi:10.5194/acp-16-1459-2016, http://
www.atmos-chem-phys.net/16/1459/2016/, 2016.

Paulot, F., Fan, S., and Horowitz, L. W.: Contrasting seasonal responses of sulfate aerosols to declining SO_2
emissions in the Eastern U.S.: Implications for the efficacy of SO_2 emission controls, Geophys. Res. Lett., 44,
455–464, doi:10.1002/2016GL070695, http://dx.doi.org/10.1002/2016GL070695, 2016GL070695, 2017.

Phoenix, G. K., Emmett, B. A., Britton, A. J., Caporn, S. J. M., Dise, N. B., Helliwell, R., Jones, L., Leake,
J. R., Leith, I. D., Sheppard, L. J., Sowerby, A., Pilkington, M. G., Rowe, E. C., Ashmore, M. R., and Power,
S. A.: Impacts of atmospheric nitrogen deposition: responses of multiple plant and soil parameters across
contrasting ecosystems in long-term field experiments, Glob. Chang. Biol., 18, 1197–1215, 2012.

Ponette-González, A. G., Weathers, K. C., and Curran, L. M.: Tropical land-cover change alters biogeochemical
inputs to ecosystems in a Mexican montane landscape, Ecol. Appl., 20, 1820–1837, 2010.

Portmann, F. T., Siebert, S., and Döll, P.: MIRCA2000 — Global monthly irrigated and rainfed crop areas
around the year 2000: A new high-resolution data set for agricultural and hydrological modeling, Global
Biogeochem. Cycles, 24, GB1011, 2010.

Pregitzer, K. S., Burton, A. J., Zak, D. R., and Talhelm, A. F.: Simulated chronic nitrogen deposition increases carbon storage in Northern Temperate forests, Global Change Biol., 14, 142–153, 2008.

635 Ran, L., Pleim, J., Song, C., Band, L., Walker, J. T., and Binkowski, F. S.: A photosynthesis-based two-leaf canopy stomatal conductance model for meteorology and air quality modeling with WRF/CMAQ PX LSM, Journal of Geophysical Research: Atmospheres, 122, 1930–1952, doi:10.1002/2016jd025583, https://doi.org/10.1002/2016jd025583, 2017.

Reay, D. S., Dentener, F., Smith, P., Grace, J., and Feely, R. A.: Global nitrogen deposition and carbon sinks,
640 Nat. Geosci., 1, 430–437, 2008.

Riahi, K., Rao, S., Krey, V., Cho, C., Chirkov, V., Fischer, G., Kindermann, G., Nakicenovic, N., and Rafaj, P.: RCP 8.5—A scenario of comparatively high greenhouse gas emissions, Clim. Chang., 109, 33–57, 2011.

Riddick, S., Ward, D., Hess, P., Mahowald, N., Massad, R., and Holland, E.: Estimate of changes in agricultural terrestrial nitrogen pathways and ammonia emissions from 1850 to present in the Community
645 Earth System Model, Biogeosciences, 13, 3397–3426, doi:10.5194/bg-13-3397-2016, https://doi.org/10.5194/bg-13-3397-2016, 2016.

Rienecker, M. M., Suarez, M. J., Gelaro, R., Todling, R., Bacmeister, J., Liu, E., Bosilovich, M. G., Schubert, S. D., Takacs, L., Kim, G.-K., Bloom, S., Chen, J., Collins, D., Conaty, A., da Silva, A., Gu, W., Joiner, J., Koster, R. D., Lucchesi, R., Molod, A., Owens, T., Pawson, S., Pegion, P., Redder, C. R., Reichle, R., Robert-
650 son, F. R., Ruddick, A. G., Sienkiewicz, M., and Woollen, J.: MERRA: NASA's Modern-Era Retrospective Analysis for Research and Applications, J. Clim., 24, 3624–3648, 2011.

Sanderson, M. G., Collins, W. J., Hemming, D. L., and Betts, R. A.: Stomatal conductance changes due to increasing carbon dioxide levels: Projected impact on surface ozone levels, Tellus B, 59, doi:10.3402/tellusb.v59i3.17002, http://www.tellusb.net/index.php/tellusb/article/view/17002, 2007.

655 Schwede, D. B. and Lear, G. G.: A novel hybrid approach for estimating total deposition in the United States, Atmos. Environ., 92, 207–220, 2014.

Sheppard, L. J., Leith, I. D., Mizunuma, T., Neil Cape, J., Crossley, A., Leeson, S., Sutton, M. A., van Dijk, N., and Fowler, D.: Dry deposition of ammonia gas drives species change faster than wet deposition of ammonium ions: evidence from a long-term field manipulation, Glob. Chang.
660 Biol., 17, 3589–3607, doi:10.1111/j.1365-2486.2011.02478.x, http://onlinelibrary.wiley.com/doi/10.1111/j.1365-2486.2011.02478.x/abstract, 2011.

Shevliakova, E., Pacala, S. W., Malyshev, S., Hurtt, G. C., Milly, P. C. D., Caspersen, J. P., Sentman, L. T., Fisk, J. P., Wirth, C., and Crevoisier, C.: Carbon cycling under 300 years of land use change: Importance of the secondary vegetation sink, Global Biogeochem. Cycles, 23, GB2022, 2009.

665 Simkin, S. M., Allen, E. B., Bowman, W. D., Clark, C. M., Belnap, J., Brooks, M. L., Cade, B. S., Collins, S. L., Geiser, L. H., Gilliam, F. S., Jovan, S. E., Pardo, L. H., Schulz, B. K., Stevens, C. J., Suding, K. N., Throop, H. L., and Waller, D. M.: Conditional vulnerability of plant diversity to atmospheric nitrogen deposition across the United States, Proc. Natl. Acad. Sci. U.S.A., 113, 4086–4091, doi:10.1073/pnas.1515241113, http://www.pnas.org/content/113/15/4086, 2016.

670 Simpson, D., Fagerli, H., Jonson, J., Tsyro, S., Wind, P., and Tuovinen, J.: The EMEP Unified Eulerian Model. Model Description. EMEP MSC-W Report 12003, The Norwegian Meteorological Institute, Oslo, Norway, 2003.

Singles, R., Sutton, M., and Weston, K.: A multi-layer model to describe the atmospheric transport and deposition of ammonia in Great Britain, Atmospheric Environment, 32, 393–399, doi:10.1016/s1352-2310(97)83467-x, https://doi.org/10.1016/s1352-2310(97)83467-x, 1998.

Smith, B., Wårlind, D., Arneth, A., Hickler, T., Leadley, P., Siltberg, J., and Zaehle, S.: Implications of incorporating N cycling and N limitations on primary production in an individual-based dynamic vegetation model, Biogeosciences, 11, 2027–2054, doi:10.5194/bg-11-2027-2014, https://doi.org/10.5194/bg-11-2027-2014, 2014.

Stevens, C. J., Dise, N. B., Mountford, J. O., and Gowing, D. J.: Impact of Nitrogen Deposition on the Species Richness of Grasslands, Science, 303, 1876–1879, 2004.

Storkey, J., Macdonald, A. J., Poulton, P. R., Scott, T., Köhler, I. H., Schnyder, H., Goulding, K. W. T., and Crawley, M. J.: Grassland biodiversity bounces back from long-term nitrogen addition, Nature, 528, 401–404, doi:10.1038/nature16444, http://www.nature.com/nature/journal/v528/n7582/abs/nature16444.html, 2015.

Sutton, M., Nemitz, E., Erisman, J., Beier, C., Bahl, K. B., Cellier, P., de Vries, W., Cotrufo, F., Skiba, U., Marco, C. D., Jones, S., Laville, P., Soussana, J., Loubet, B., Twigg, M., Famulari, D., Whitehead, J., Gallagher, M., Neftel, A., Flechard, C., Herrmann, B., Calanca, P., Schjoerring, J., Daemmgen, U., Horvath, L., Tang, Y., Emmett, B., Tietema, A., Peñuelas, J., Kesik, M., Brueggemann, N., Pilegaard, K., Vesala, T., Campbell, C., Olesen, J., Dragosits, U., Theobald, M., Levy, P., Mobbs, D., Milne, R., Viovy, N., Vuichard, N., Smith, J., Smith, P., Bergamaschi, P., Fowler, D., and Reis, S.: Challenges in quantifying biosphere–atmosphere exchange of nitrogen species, Environmental Pollution, 150, 125–139, doi:10.1016/j.envpol.2007.04.014, https://doi.org/10.1016/j.envpol.2007.04.014, 2007.

Sutton, M. A., Simpson, D., Levy, P. E., Smith, R. I., Reis, S., Van Oijen, M., and De Vries, W.: Uncertainties in the relationship between atmospheric nitrogen deposition and forest carbon sequestration, Glob. Chang. Biol., 14, 2057–2063, 2008.

Sutton, M. A., Howard, C. M., Erisman, J. W., Billen, G., Bleeker, A., Grennfelt, P., Grinsven, H. v., and Grizzetti, B., eds.: The European Nitrogen Assessment: Sources, Effects and Policy Perspectives, Cambridge University Press, 2011.

Templer, P. H., Weathers, K. C., Lindsey, A., Lenoir, K., and Scott, L.: Atmospheric inputs and nitrogen saturation status in and adjacent to Class I wilderness areas of the northeastern US, Oecologia, 177, 5–15, 2014.

Townsend, A. R., Braswell, B. H., Holland, E. A., and Penner, J. E.: Spatial and Temporal Patterns in Terrestrial Carbon Storage Due to Deposition of Fossil Fuel Nitrogen, Ecol. Appl., 6, 806–814, 1996.

Tulloss, E. M. and Cadenasso, M. L.: Nitrogen deposition across scales: hotspots and gradients in a California savanna landscape, Ecosphere, 6, art167, doi:10.1890/es14-00440.1, https://doi.org/10.1890/es14-00440.1, 2015.

Vieno, M., Dore, A. J., Wind, P., Marco, C. D., Nemitz, E., Phillips, G., Tarrasón, L., and Sutton, M. A.: Application of the EMEP Unified Model to the UK with a Horizontal Resolution of 5x 5 km2, in: Atmospheric Ammonia, pp. 367–372, Springer Netherlands, doi:10.1007/978-1-4020-9121-6_21, https://doi.org/10.1007/978-1-4020-9121-6_21, 2009.

Wang, Y., Jacob, D. J., and Logan, J. A.: Global simulation of tropospheric O_3-NO_x-hydrocarbon chemistry 1. Model formulation, J. Geophys. Res., 103, 10 713–10 726, 1998.

Wårlind, D., Smith, B., Hickler, T., and Arneth, A.: Nitrogen feedbacks increase future terrestrial ecosystem carbon uptake in an individual-based dynamic vegetation model, Biogeosciences, 11, 6131–6146, 2014.

715 Weathers, K. C., Lovett, G. M., Likens, G. E., and Lathrop, R.: The Effect of Landscape Features on Deposition to Hunter Mountain, Catskill Mountains, New York, Ecol. Appl., 10, 528–540, doi:10.2307/2641112, http://www.jstor.org/stable/2641112, 2000.

Weathers, K. C., Simkin, S. M., Lovett, G. M., and Lindberg, S. E.: Empirical Modeling of Atmospheric Deposition in Mountainous Landscapes, Ecol. Appl., 16, 1590–1607, 2006.

720 Wentworth, G. R., Murphy, J. G., Benedict, K. B., Bangs, E. J., and Collett Jr., J. L.: The role of dew as a night-time reservoir and morning source for atmospheric ammonia, Atmos. Chem. Phys., 16, 7435–7449, doi:10.5194/acp-16-7435-2016, http://www.atmos-chem-phys.net/16/7435/2016/, 2016.

Wesely, M. . L.: Parameterization of surface resistances to gaseous dry deposition in regional-scale numerical models, Atmos. Environ., 23, 1293–1304, 1989.

725 Williams, J. J., Chung, S. H., Johansen, A. M., Lamb, B. K., Vaughan, J. K., and Beutel, M.: Evaluation of atmospheric nitrogen deposition model performance in the context of U.S. critical load assessments, Atmospheric Environment, 150, 244–255, doi:10.1016/j.atmosenv.2016.11.051, https://doi.org/10.1016/j.atmosenv.2016.11.051, 2017.

Wolfe, A. P., Van Gorp, A. C., and Baron, J. S.: Recent ecological and biogeochemical changes in alpine
730 lakes of Rocky Mountain National Park (Colorado, USA): a response to anthropogenic nitrogen deposition, Geobiology, 1, 153–168, 2003.

Wu, W. and Driscoll, C. T.: Impact of Climate Change on Three-Dimensional Dynamic Critical Load Functions, Environ. Sci. Technol., 44, 720–726, pMID: 20020745, 2010.

Wu, Z., Staebler, R., Vet, R., and Zhang, L.: Dry deposition of O_3 and SO_2 estimated from gradient measure-
735 ments above a temperate mixed forest, Environ. Pollut., 210, 202–210, doi:10.1016/j.envpol.2015.11.052, http://www.sciencedirect.com/science/article/pii/S0269749115302128, 2016.

Wu, Z., Schwede, D. B., Vet, R., Walker, J. T., Shaw, M., Staebler, R., and Zhang, L.: Evaluation and intercomparison of five North American dry deposition algorithms at a mixed forest site, Journal of Advances in Modeling Earth Systems, doi:10.1029/2017ms001231, https://doi.org/10.1029/2017ms001231, 2018.

740 Zaehle, S., Friend, A. D., Friedlingstein, P., Dentener, F., Peylin, P., and Schulz, M.: Carbon and nitrogen cycle dynamics in the O-CN land surface model: 2. Role of the nitrogen cycle in the historical terrestrial carbon balance, Global Biogeochemical Cycles, 24, n/a–n/a, doi:10.1029/2009gb003522, https://doi.org/10.1029/2009gb003522, 2010.

Zhang, L., Gong, S., Padro, J., and Barrie, L.: A size-segregated particle dry deposition scheme for an atmo-
745 spheric aerosol module, Atmos. Environ., 35, 549–560, 2001.

Zhang, L., Moran, M. D., Makar, P. A., Brook, J. R., and Sunling, G.: Modelling gaseous dry deposition in AURAMS: a unified regional air-quality modelling system, Atmos. Environ., 36, 537—560, 2002.

Zhang, L., Brook, J. R., and Vet, R.: A revised parameterization for gaseous dry deposition in air-quality models, Atmos. Chem. Phys., 3, 2067–2082, 2003.

750 Zhang, L., Jacob, D. J., Knipping, E. M., Kumar, N., Munger, J. W., Carouge, C. C., van Donkelaar, A., Wang, Y. X., and Chen, D.: Nitrogen deposition to the United States: distribution, sources, and processes, Atmos. Chem. Phys., 12, 4539–4554, 2012.

Zhu, L., Henze, D., Bash, J., Jeong, G.-R., Cady-Pereira, K., Shephard, M., Luo, M., Paulot, F., and Capps, S.: Global evaluation of ammonia bidirectional exchange and livestock diurnal variation schemes, Atmos. Chem. Phys., 15, 12 823–12 843, doi:10.5194/acp-15-12823-2015, http://www.atmos-chem-phys.net/15/12823/2015/, 2015.